Internal note nr 1
Pham Ngoc Dinh + Pierre Darriulat
November 2000

Scintillation Counters Calibration

1 Introduction

Eighteen scintillator plates (formerly used in the CHARM 2 experiment) have been equipped with 12-dynodes 2" photomultiplier tubes (AVP56 or equivalent, from College de France and various other origins) in preparation for their installation in the Auger training bench. Prior to installation the response of each detector to cosmic muons has been measured. The main results are presented below.

2 Description of the test setup

The plates under test were first examined for possible major and obvious faults, such as big light leaks, broken light guides, etc. The light guides are simply 15cm long, 4cm in diameter lucite cylinders glued in the middle of one of the shorter plate sides. When they were missing or broken they were reglued in the middle of the opposite side after proper polishing. The phototubes and phototube bases were also checked for major faults and either fixed or, when they could not be fixed, discarded. The linear voltage dividers were checked for proper operation and the relative values of the focusing electrode voltage were adjusted by scope inspection.

A cosmic trigger was defined by a threefold coincidence between scintillator counters accepting cosmic particles over a cone of 2.5 steradians approximate aperture. Two $6\times6\text{cm}^2$ overlapping scintillators define the cone apex and a standard $120\times40\times3\text{cm}^3$ plate defines the base in the geometry of Figure 1. The scintillator plate being tested is positioned just above the cone apex, parallel to the base plate, and can be moved in the x or y directions in order for the trigger particles to shine different spots.

The test setup electronics is sketched in Figure 2. The fast trigger logics uses standard NIM units from the CERN Electronics Pool. Each anode signal is split (passively) into two equal pulses, one feeding a fast discriminator at the input of the trigger circuitry, the other being sent through a 50Ω, 120ns delay cable to a 10 bit LRS 2249A analog to digital converter (ADC)

for pulse height analysis. The final trigger coincidence includes, in addition to the trigger counter signals, an adjustable dead time. The linear output of the coincidence is used to generate the 100ns wide ADC gate with respect to which the anode pulses have been carefully timed. Data acquisition is made under CAMAC and uses a CC7700 CAMAC crate controller (from RIKEN) interfaced to a FT 3601-00 PC running Linux standard software (the user routines being written in C language). The data are organized and histogrammed under PAW, both online or offline. Readout is initiated whenever a LookAtMe (LAM) signal is present on the ADC line, which occurs when a pulse height in excess of a preset threshold is present on one of the ADC inputs within the ADC gate. In order to avoid hang-ups caused by the occasional occurrence of LAMless gates (very low pulse heights at the ADC inputs) the gate signal itself is digitized in one of the ADC channels.

All phototube signals were digitized and recorded. A few pulse height spectra are shown in Figure 3. They include the three trigger counters as well as a few other counters which were located (for part of the study) between the apex trigger counters and the base plate. In all cases a spectrum characteristic of minimum ionizing muons is visible and provides evidence for proper operation of the system, including the settings of the discriminator thresholds, of the ADC pedestals, etc.

The stability over the three weeks during which the test was run was excellent and the trigger rate was consistent with expectation.

3 Results

Spectra measured in the center of the plates

Two typical spectra ($x = 0$) are shown in Figure 4 and are compared with the result of a simulation (see below). Tables 1a and 1b list the mean and rms values of the spectra measured along the central line of each plate ($y = 0$). Typical statistical uncertainties are of the order of a few percent for both the mean and the rms but important systematic uncertainties are present at large x values, near the light guide, as a result of the uncertainty on setting x in a region where the pulse height varies rapidly. This effect is clearly visible in Figure 5 below where it is responsible for the important spread between the large x data.

Longitudinal scans ($y = 0$)

Each plate was scanned in x in 10cm steps along the $y = 0$ axis.

The counters were found to belong to one of three types:

Type 1, including nine counters, exhibits a spectrum characteristic of a

homogeneous scintillator plate. The result of the scans is shown in Figure 5. A simple Monte Carlo program has been written to simulate the mechanism of light collection in such a plate. The relevant parameters are the photocathode efficiency k, the attenuation length λ_{att}, the refraction index n and a reflection parameter ϵ measuring the fraction of the light actually reflected at each total reflection (the light that is not totally reflected is considered to be lost, diffusion is ignored). A fair description of the data is obtained using sensible values of the parameters: $k = 10$ % , $\lambda_{att} = 5$ m, $n = 1.55$, $\epsilon = 0.995$, and assuming a scintillation yield of 700 photons per mm, taken about three times lower than for a very good scintillator in order to account for ageing. No attempt was made at fitting the parameters in the present crude comparison. Such fits will require scans over the whole plate area and a better muon selection. They will be performed later on *in situ*. The simulation shows that full efficiency is expected over the whole plate. For each central muon normally incident on the plate there are, on average, ~100 photons (i.e. 10 photoelectrons) which make their way to the phototube. Again on average, each of these has a path length of ~3m in the scintillator and suffers ~40 reflections.

Types 2 and 3 exhibit a step at a distance of 40cm from one of the shorter plate edges, beyond which the counter response falls essentially to zero, as illustrated in Figure 6 and 7. In the case of Type 2 (five counters) the step is located on the light guide side, in the case of Type 3 it is located on the opposite side. The reason is that these plates are in fact made of a 80×40cm^2 scintillator plate glued onto a 40×40cm^2 lucite plate. Originally the light guide was located on the lucite side, as it should, but when it was missing or broken it had been reglued on the opposite side. The four Type 3 counters will be modified to have the light guide reglued on the lucite plate, near the middle of the shorter side but slightly off center if considered necessary to secure a good surface polish.

4 Conclusion

The test has shown the proper performance of the whole setup and the good control we have over its operation. Scintillators are of excellent quality and can be used to assemble the trigger/tagging system of the final test bench detector. We propose to use the nine counters of Type 1 arranged in three planes of 120×120cm^2 below the Cerenkov counter and eight counters of Type 2 arranged in two planes of 160×80cm^2 above the Cerenkov counter (this leaves one counter of Type 2 as a spare; note that after modification

of Type 3 as described above all such counters will belong to Type 2).

In this way, both the upper and lower planes will be effectively segmented into $40\times40\text{cm}^2$ squares (nine such squares below and eight above the Cerenkov counter).

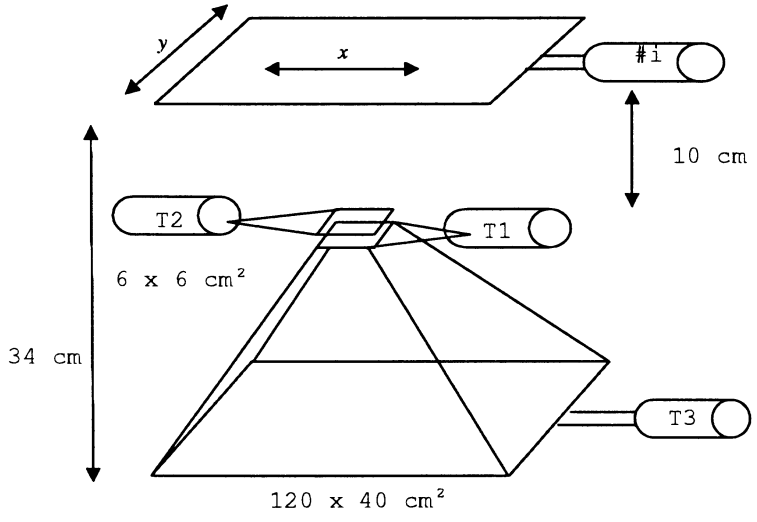

Figure 1: Geometry of the calibration set up. A triple coincidence between T1, T2, and T3 defines the trigger. Counter # i is the counter under study (scanned along x at $y = 0$).

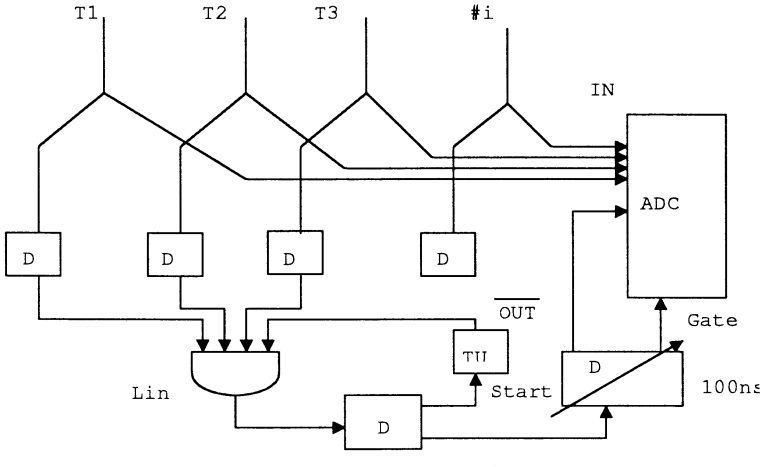

Figure 2: Simplified diagram of the electronics. Discriminators D are 20ns wide except for that defining the ADC gate which is 100ns wide. A timing unit (TU) is used to introduce a dead time of a few ms.

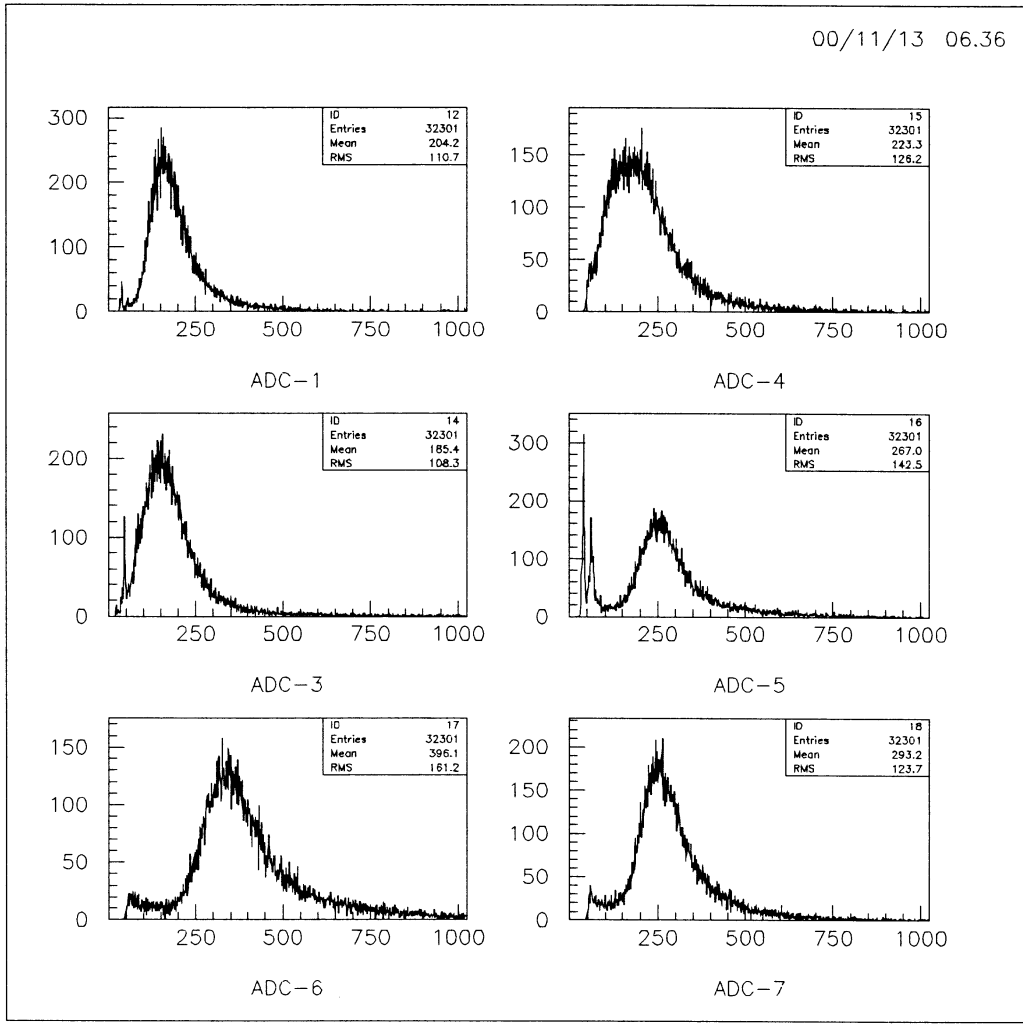

Figure 3: Pulse height distributions of different counters: the top two spectra are of standard plates not included in the trigger, the bottom two spectra are of the trigger cross counters. The middle spectra are of the trigger base plate (left) and the cross counter not included in the trigger (right).

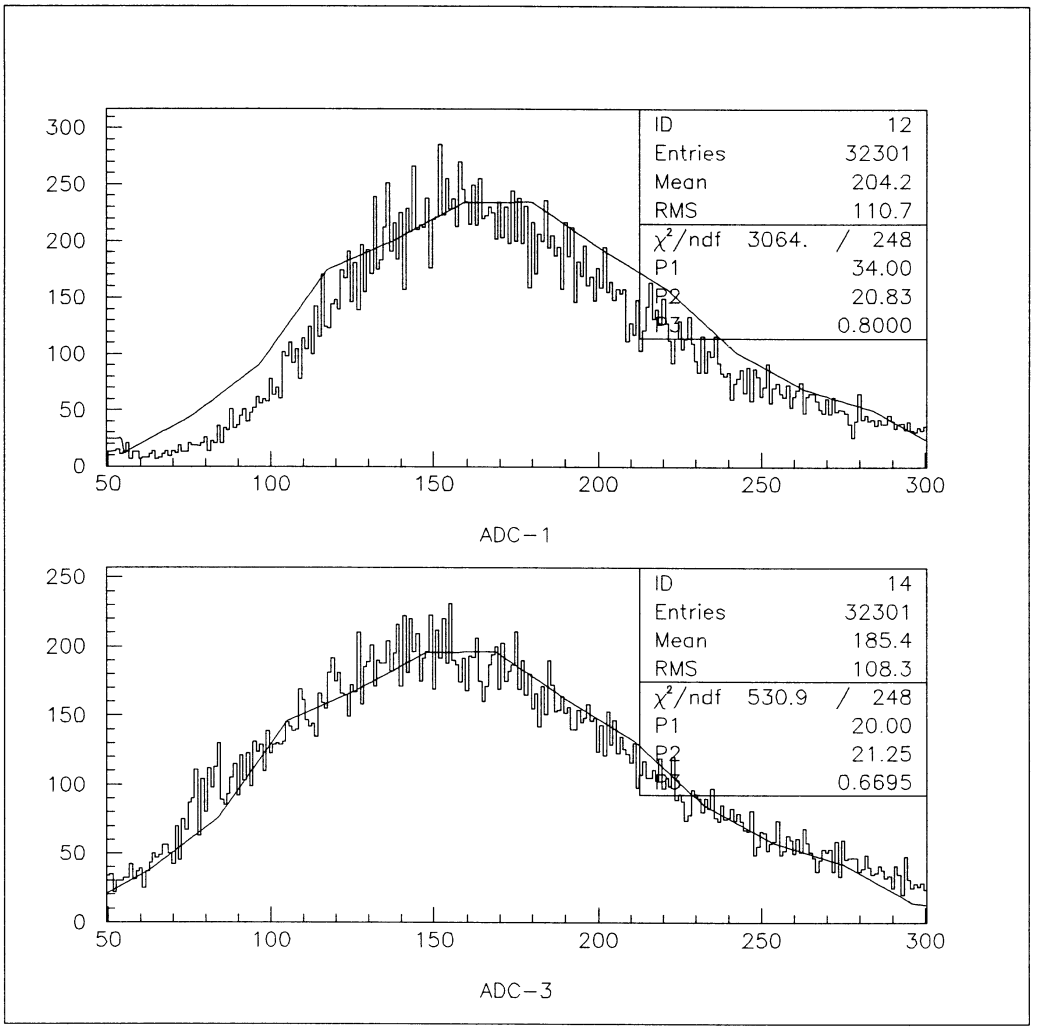

Figure 4: Pulse height distributions of a counter located close to the cross (top) and of the trigger base plate (bottom). The line is the result of the Monte Carlo calculation where the abscissae has been scaled to approximately fit the data.

Table 1a. The mean values of the pulse height spectra measured for each counter (counter labels are given in column 1) at $y = 0$ and various x positions (given on the top line in cm). Counters have been grouped according to their type.

Type 1

	-50	-40	-30	-20	-10	0	10	20	30	40	50
1	179	199	182	212	201	163	183	207	252	321	394
4	189	196	209	225	220	233	231	0	282	374	474
5	163	177	179	180	180	176	196	235	254	340	379
6	178	173	196	174	206	194	200	206	226	283	370
8	162	186	186	167	191	205	214	198	238	284	401
13	161	175	171	184	204	200	188	209	243	242	250
14	175	199	185	194	227	185	201	207	204	240	273
15	181	181	202	195	183	207	195	194	223	298	417
17	165	182	173	189	194	190	191	197	265	302	375

Type 2

	-50	-40	-30	-20	-10	0	10	20	30	40	50
2	198	210	202	230	232	243	254	175	64	63	65
10	201	215	214	190	257	255	252	163	69	57	67
11	198	213	210	209	239	238	239	188	77	73	70
12	208	214	242	251	226	231	214	146	89	75	73
18	223	217	231	219	201	249	260	174	64	62	74

Type 3

	-50	-40	-30	-20	-10	0	10	20	30	40	50
3	51	66	82	134	198	195	216	271	303	344	292
7	52	55	63	123	246	226	235	253	255	311	374
9	62	68	76	154	209	221	232	242	266	341	473
16	70	67	93	133	202	241	235	235	261	274	264

Table 1b. The rms values the pulse height spectra measured for each counter (counter labels in column 1) at $y = 0$ and various x positions (given on the top line in cm). Counters have been grouped according to their type.

Type 1

	-50	-40	-30	-20	-10	0	10	20	30	40	50
1	76	106	84	116	96	96	94	105	121	137	151
4	111	87	105	126	114	124	87	0	110	154	206
5	94	126	105	103	118	109	95	135	114	163	201
6	97	91	131	103	124	96	109	118	106	126	182
8	105	128	112	108	123	126	146	90	137	138	195
13	105	104	95	112	126	122	100	137	141	134	184
14	154	149	117	149	169	118	126	147	142	165	208
15	142	128	161	152	128	158	143	132	160	177	125
17	86	116	88	135	126	91	104	96	155	166	188

Type 2

	-50	-40	-30	-20	-10	0	10	20	30	40	50
2	100	122	98	137	127	136	131	108	66	58	67
10	106	101	136	107	140	147	129	156	117	80	89
11	109	107	88	88	114	116	93	140	111	102	93
12	159	136	133	139	134	140	144	125	114	99	93
18	116	103	138	99	151	136	127	145	90	51	76

Type 3

	-50	-40	-30	-20	-10	0	10	20	30	40	50
3	66	85	102	124	136	116	106	140	184	178	214
7	71	63	86	109	147	105	123	117	99	109	159
9	49	90	92	132	100	114	136	126	146	140	211
16	78	57	108	102	150	133	133	107	160	184	206

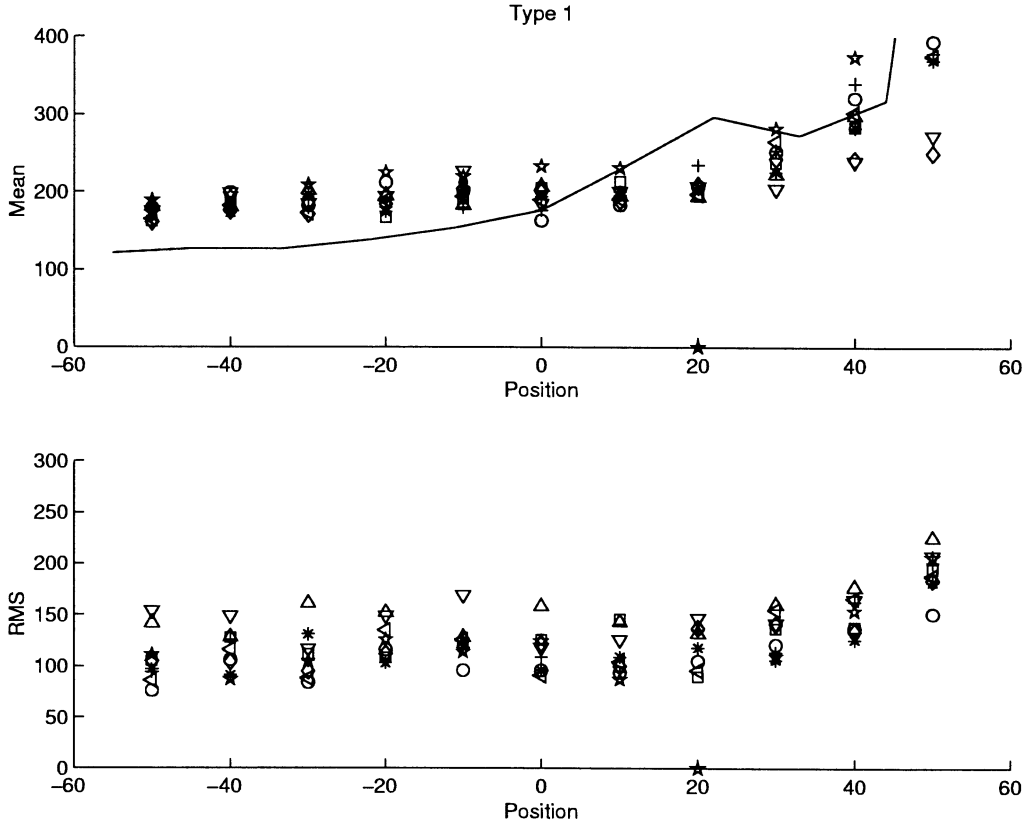

Figure 5: The mean of the pulse height distribution (top) and its rms value (bottom) as a function of x (cm) at $y = 0$ for all counters of type 1. The data of each counter have been normalized to have a mean pulse height value of 200 channels for x between $\pm$ 30 cm.The curve is the result of the Monte Carlo simulation (see text).

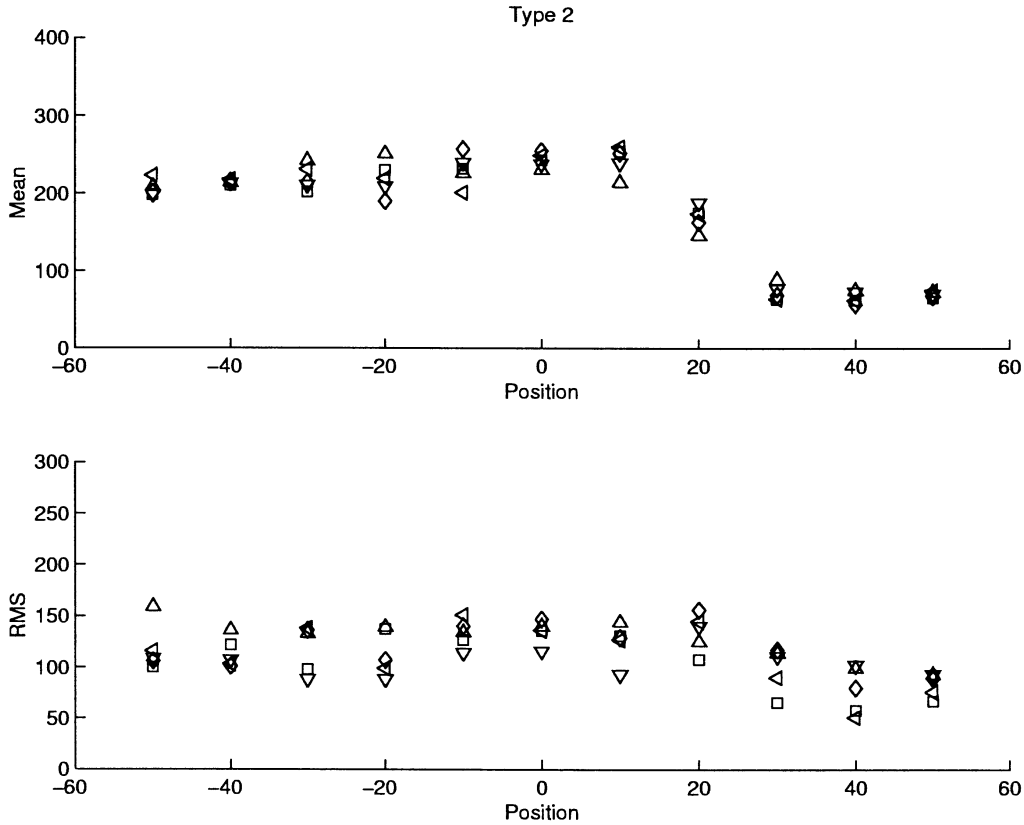

Figure 6: The mean of the pulse height distribution (top) and its rms value (bottom) as a function of x (cm) at $y = 0$ for all counters of type 2. The data of each counter have been normalized to have a mean pulse height value of 200 channels for x between $\pm$ 30 cm.

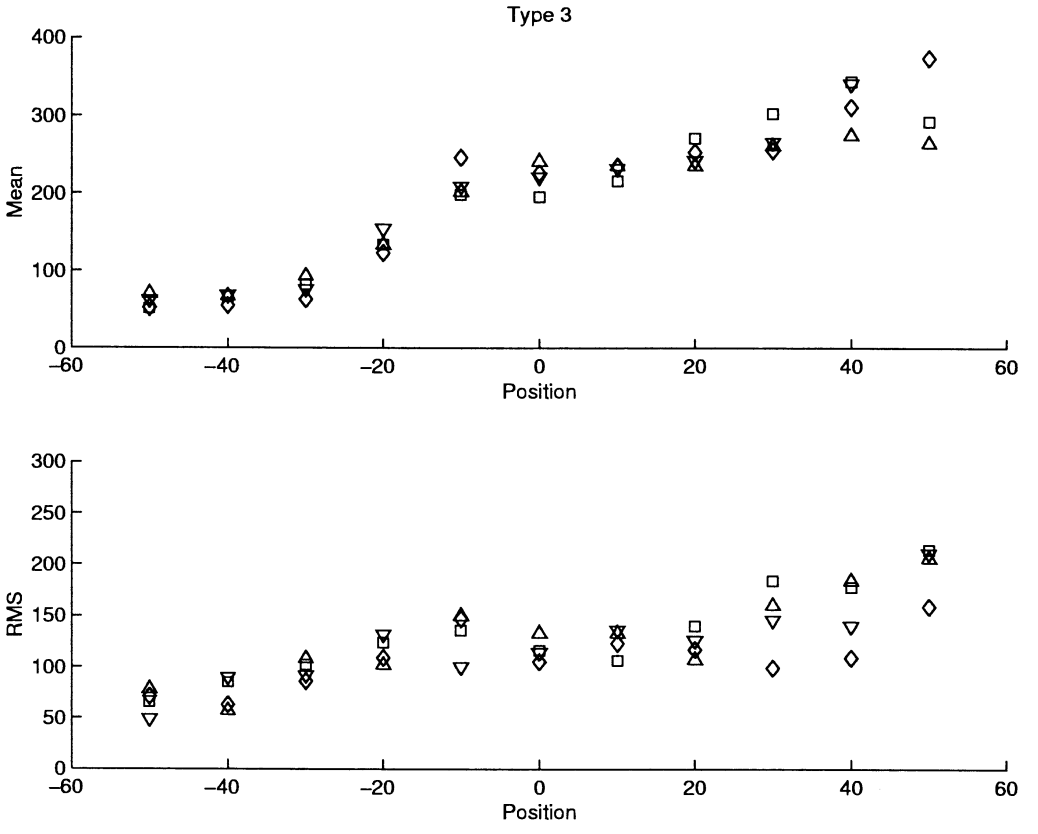

Figure 7: The mean of the pulse height distribution (top) and its rms value (bottom) as a function of x (cm) at $y = 0$ for all counters of type 3. The data of each counter have been normalized to have a mean pulse height value of 200 channels for x between $\pm$ 30 cm.